Accepted Manuscript

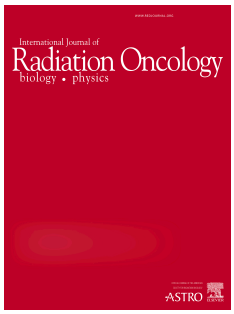

Experimental studies of boronophenylalanine (^{10}BPA) biodistribution for the individually tailored application of boron neutron capture therapy (BNCT) for malignant melanoma treatment

M. Carpano, M. Perona, C. Rodriguez, S. Nievas, M. Olivera, G.A. Santa Cruz, D. Brandizzi, R. Cabrini, M. Pisarev, G. Juvenal, M.A. Dagrosa

PII: S0360-3016(15)00601-X

DOI: 10.1016/j.ijrobp.2015.05.039

Reference: ROB 22939

To appear in: *International Journal of Radiation Oncology • Biology • Physics*

Received Date: 12 February 2015

Revised Date: 16 May 2015

Accepted Date: 26 May 2015

Please cite this article as: Carpano M, Perona M, Rodriguez C, Nievas S, Olivera M, Santa Cruz GA, Brandizzi D, Cabrini R, Pisarev M, Juvenal G, Dagrosa MA, Experimental studies of boronophenylalanine (^{10}BPA) biodistribution for the individually tailored application of boron neutron capture therapy (BNCT) for malignant melanoma treatment, *International Journal of Radiation Oncology • Biology • Physics* (2015), doi: 10.1016/j.ijrobp.2015.05.039.

Experimental studies of boronophenylalanine (^{10}BPA) biodistribution for the individually tailored application of boron neutron capture therapy (BNCT) for malignant melanoma treatment

M. Carpano[1], M. Perona[1], C. Rodriguez[1], S. Nievas[2], M. Olivera[2], G.A. Santa Cruz[2], D. Brandizzi[1,3], R. Cabrini[1,3], M. Pisarev [1,4,5], G. Juvenal[1,4] , M.A. Dagrosa [1,4]

[1]Dept Radiobiology; [2]Dept of BNCT, National Atomic Energy Commission (CNEA), Av. General Paz 1499, (1650) San Martín, Argentina.

[3]School of Dentistry, University of Buenos Aires, M.T. De Alvear 2142, (1121) Ciudad Autónoma de Buenos Aires, Argentina.

[4]National Research Council of Argentina (CONICET), Rivadavia 1917, (1033) Ciudad Autónoma de Buenos Aires, Argentina.

[5]Dept of Human Biochemistry, School of Medicine, University of Buenos Aires, Paraguay 2155, (1121) Ciudad Autónoma de Buenos Aires, Argentina.

Corresponding author: dagrosa@cnea.gov.ar

Running Title: Individual application of BNCT for melanoma

Keywords: BPA, uptake, individual, melanoma, infrared imaging

Notes: The authors declare that they have no conflict of interest.

Alejandra Dagrosa and Guillermo Juvenal should be considered as joint authors

Summary

The aim of the present studies was to evaluate the biodistribution of boronophenilalanina (^{10}BPA) for the potential application of BNCT for the treatment of melanoma on an individual basis. A significant correlation between tumor temperature and tumor-to-blood (T/B) boron concentration ratio was found. A high number of positive cells for the proliferation marker Ki-67 and blood vessels of large diameter evidenced by the endothelial marker CD31 was observed in tumors with the higher T/B ratios.

Experimental studies of boronophenylalanine (^{10}BPA) biodistribution for the individual application of boron neutron capture therapy (BNCT) for malignant melanoma treatment

XXXX[1], XXXX[1], XXXX[1], XXXX[2], XXXX[2], XXXX[2], XXXX[1,3], XXXX[1,3], XXXX [1,4,5], XXXX[1,4] , XXXX [1,4]

[1]XXXX; [2]XXXX, XXXX.

[3]XXXX, XXXX.

[4]XXXX.

[5]XXXX, XXXX.

Running Title: Individual application of BNCT for melanoma

Abstract

Purpose: Patients with the same histopathological diagnosis of cutaneous melanoma treated with identical protocols of boron neutron capture therapy (BNCT), have shown different clinical outcomes. The objetive of the present studies was to evaluate the biodistribution of boronophenilalanina (^{10}BPA) for the potential application of BNCT for the treatment of melanoma on an individual basis. Methods and Materials: The boronophenilalanine (BPA) uptake was evaluated in three human melanoma cell lines MEL-J, A375 and M8. NIH nude mice were implanted with 4 10^6 MEL-J cells and biodistribution studies of BPA (350mg/kg i.p) were performed. Static Infrared Imaging (SIRI) utilizing a specially modified infrared camera adapted to measure the body infrared radiance of small animals, was employed. Proliferation marker, Ki-67 and endothelial marker, CD31, were analysed in tumor samples. Results: The in vitro studies demonstrated different patterns of boronophenilalanine (BPA) uptake for each analysed cell line (*** $p < 0.001$ for MEL-J and A375 vs. M8 cells). The in vivo studies showed a maximum average boron concentration of 25.9 ± 2.6 µg/g in tumor, with individual values ranging between 11.7 and 52.0 µg/g of ^{10}B at 2 h post-injection of BPA. Tumor temperature always decreased as the tumors increased in size, with values ranging between 37 ºC and 23 ºC. A significant correlation between tumor temperature and tumor-to-blood boron concentration ratio was found (R-square=0.7, rational function fit). The immunohistochemical studies revealed, in tumors with extensive areas of viability, a high number of positive cells for Ki-67, blood vessels of large diameter evidenced by the marker CD31 and a direct logistic correlation between proliferative status and boron concentration difference between tumor and blood (R-square=0.81, logistic function fit). Conclusion: We propose that these methods could be suitable for designing new screening protocols applied prior to melanoma BNCT treatment for each individual patient and lesion.

1. Introduction

Malignant melanoma is one of the most aggressive cancers in humans and is responsible for almost 60% of all lethal skin tumors. The incidence of melanoma has been increasing in white population in the past two decades. There is a complex interaction

between environmental (exogenous) and endogenous risk factors, in developing malignant melanoma. Usually it can be controlled with conventional or standard treatments if its detection occurs in the early stages of the disease. However, when the tumor is in an advanced stage, the effectiveness of these therapies is poor (1).

Boron neutron capture therapy (BNCT) is considered a radiation therapy technique based on the selective uptake of a boron compound by tumoral tissue in comparison to surrounding normal tissue. Once the appropriated concentration of boron is achieved, the tumor is irradiated with a thermal or epithermal neutron beam. Following neutron capture, the unstable ^{11}B nucleus immediately decays and releases an alpha particle and a ^{7}Li nucleus. These high Linear Energy Transfer (LET) particles cause chromatin damage, difficult to repair and prone to create lethal lesions (2). At present, neutron sources for BNCT are currently limited to nuclear reactors, and clinical trials are being performed in several countries including Italy, Taiwan, Japan, Finland and Argentina for those malignancies that do not respond to standard therapies (3).

Since the first applications, the clinical interest in BNCT has been focused on the treatment of high grade cutaneous melanoma. Mishima et al. had previously carried out extensive experimental studies using enriched ^{10}B boronophenylalanine (BPA) (4). The first melanoma patients were treated in the USA in 1985 (5). Several other patients with either cutaneous or metastatic melanoma to the brain have been treated in other countries including Argentina (6, 7). All the results showed that BNCT seemed to be suitable to treat metastases of superficial cutaneous melanoma.

Histologically similar tumors may have different prognoses and may respond to the same therapy in different ways. It is believed that these differences in clinical behavior are related to molecular and structural differences between histologically similar tumors (8). At the present time, personalized medicine represents a new approach in the field of health care, that take into account the individual's clinical, genomic and genetic characteristics and the environmental factors for each patient (9). This could enable a better approach to cancer treatment and could also have the potential to achieve measurable improvements in outcomes and a reduction on health care costs.

In the present work we performed in vitro and in vivo analysis to evaluate the boron tumor incorporation for the potential application of BNCT for the treatment of cutaneous melanoma on an individual basis. In order to investigate the extent of this approach, the correlation between tumor boron uptake and different biological and physical parameters of the tumors was evaluated. Among the latter, and aiming at providing a non-invasive methodology for first-screening melanoma patients, we have employed Static Infrared Imaging (SIRI) utilizing a specially modified infrared camera adapted to measure the body infrared radiance of small animals, studying their body temperature distribution including normal, peritumoral and tumoral regions.

2. Methods and Materials

Cell lines

The human melanoma cell line MEL-J, kindly provided by Dr. José Mordoh, Instituto de Investigaciones Bioquímicas Leloir (Buenos Aires, Argentina) (10), and the human melanoma cell line M8 were cultured in RPMI1640 medium supplemented with 10%

fetal bovine serum (FBS), streptomycin (100 mg/ml) and penicillin (100 IU/ml). The human melanoma cell line A375 was cultured in DMEM/F12 medium supplemented with 10% FBS, streptomycin (100 mg/ml) and penicillin (100 IU/ml). Both cell lines were maintained at 37 °C in a humidified atmosphere containing 5% CO_2.

Animal model

NIH nude mice, aged 6 to 8 weeks and weighing 20 to 25 g were implanted (s.c.) in the back right flank with $4x10^6$ cells of the human melanoma cell line MEL-J. Animals were bred and maintained under aseptic conditions (11).

Tumor growth measurement

The size of the tumors was measured with a caliper twice a week and the volume was calculated according to the following formula: $A^2xB/2$ (were A is the width and B is the length) (12).

BPA-Fructose complex preparation

The solution of L-p boronophenylalanine (BPA) (Gliconix Corp; Durham, US) was prepared at a concentration of 30 mg ^{10}BPA per milliliter (0.14 M). Briefly, ^{10}BPA (99% ^{10}B-enriched) L-isomer, was combined in water with a 10% molar excess of fructose. The pH was adjusted to 9.5-10 with NaOH, the mixture was stirred until all solids were dissolved and the pH was then readjusted to 7.4 with HCl (13).

Experimental design

In vitro studies: Cells in exponential growth phase were used to determine the uptake of ^{10}B. The cells were incubated in 10 cm diameter petri dishes for 0.5, 2, 4 and 24 h with boronophenylalanine (BPA) (50 ppm ^{10}B). At the end of the incubation with BPA the cells were washed three times with cold PBS, harvested with trypsin and centrifuged at 900 x *g*. The number of cells was counted with a Neubauer's chamber. BPA uptake was measured by inductively-coupled plasma optical emission spectroscopy (ICP-OES) and expressed as µg/g of tissue.

Static Infrared Imaging

Body temperature mapping of living subjects requires following standard procedures that aim at minimizing the influence of ambient and physiological factors which could interfere with the desired observations. Achieving normostatic conditions is a prerequisite for live screening and it is usually accomplished by controlling ambient temperature, infrared sources and unwanted stress of the subject of observation (14).

The camera employed was a Raytheon PalmIR 250 (L3 Comm. Systems), which uses uncooled infrared ferroelectric sensors distributed in an array of 320x240 detectors, sensitive to infrared radiation in the 7-14 micrometers wavelength band. The original optics was modified from its original focus distance to observe targets located between 0.5 m and 1 m. In this way, and focusing at 0.65 m, an angular field of view of 11°x8° and spatial resolution of 0.39 mm/pixel were achieved. Total temperature resolution, which comprises both the intrinsic sensitivity above noise and rounding by the analog-to-digital conversion procedure, was about 0.3°C. The camera provides also an NTSC video signal that can be employed for studying temperature evolution (as needed in Dynamic Infrared Imaging, or DIRI, studies) or to improve S/N Ratios by averaging video frames.

The infrared camera is routinely calibrated in temperature by reference black bodies. The assumed emissivity is 0.98 (a typical value for normal skin). To reduce changes in the mice homeostasis, the room is kept at a stable temperature, between 22 and 23 ºC. A set of 10 mice were examined with SIRI twice a week, during approximately 40 days after s.c. inoculation of tumor cells. For the studies, mice were held by hand without anesthesia and infrared videos were acquired for a few seconds in order to avoid the stressing influence of the immobilization procedure in the animal's body temperature. Short videos were acquired for each mouse observing the right (inoculated side) and left flanks (normal side), and groin temperature was measured with a thermocouple as representative of body core temperature. All the SIRI studies were performed before BPA administration and animal sacrifice, thereby serving as an *a priori* non-invasive screening method.

In vivo studies: To evaluate the BPA uptake, animals were injected with the boron compound at a dose of 350 mg/Kg b.w. (i.p.) and sacrificed at 0.5, 1, 2 and 3 h post-administration. A total of 12 biodistribution studies were performed and 10 mice per group were used. For boron determination, tissue samples were always weighed before digestion. The tumor samples were divided into two pieces: one for boron measurement and the other for histological analysis. For histology and immunohistochemistry analyses, a rectangular band (300 x 6400 µm) in the sample preparation, which includes the entire tumor growth region, was analysed.

Boron measurements

Digestion of tissue samples, with a mass range of 10-50 mg, was carried out for 2 h at 60°C with 0.15 ml of a 1:1 mixture of concentrated nitric and sulfuric acids. Dilution to 1.0 ml was performed with 0.65 ml of a 5% aqueous solution of Triton X-100 (v/v) and 0.2 ml of a solution containing 25 μg/ml Sr and 0.5μg/ml Y as internal standards. Blood samples (200-300 μl) were digested for 2 h at the same temperature with 1.0 ml of the 1:1 acid mixture and diluted to 5.0 ml with 3.0 ml of the Triton X-100 and 1.0 ml of the internal standard solution. Analytical and internal standard lines (in nm) were as follows: B: 249.677; Sr: 232.235; and Y: 371.029. Matrix matched standard solutions containing the internal standard elements and boron between 0.05 and 1.0 μg/ml were employed for daily calibration.

Hematoxylin and Eosin (H&E) stains and immunohistochemistry

Histological preparations were prepared from the tumor and the surrounding skin. Briefly, tissues were fixed with 10% buffered formol (pH 7.0) and paraffin embedded. Ten-micron-thick sections were cut and stained with H&E. All sections for immunohistochemistry were deparaffinized and rehydrated using graded concentrations of ethanol prepared with deionized water. The slides were transferred into a 0.05 M Tris-based solution in 0.15 M NaCl with 0.1% v/v Triton-X-100, pH 7.6 (TBST). Endogenous peroxidase was blocked with 3% hydrogen peroxide for 10 min. Antigen retrieval was done using microwave in citrate buffer at pH 6.0. All slides were incubated at room temperature for 1 h with one of two antibodies: rabbit polyclonal antibody against CD31, a validated endothelial marker (Abcam, Cambridge, UK) or monoclonal mouse anti-rat Ki-67, a marker of cell proliferation (DAKO, Ely, UK). Using a kidney and liver sections as controls, the highest titer of primary antibodies to produce optimal demonstration of microvessels with the lowest acceptable background

staining was 1:50 for both anti CD31 and Ki-67. Negative controls were obtained by eliminating the primary antibodies from the diluents. After washing with PBS-Tween, biotinylated goat anti-rabbit IgG (1:1000; Cell Marque) was applied to the sections for 30 minutes at room temperature. Sections were then incubated with Strepavidin -HRP (Sigma) for 30 minutes at room temperature. Diaminobenzide (DAB) was used as the cromagen and hematoxylin as the counterstain. Immunohistochemistry quantitation was performed by combining image and computerized microspectrophotometric analysis (15). Digital images were obtained from a single field of the preparation using a Zeiss MPM 400 microscope with an objective x 20/0, 75 a. Densitometric measurements were done with an image analysis program. The analysis was performed in 7 cases. The following parameters were evaluated in each case: total field area, number of Ki-67 or CD31 positive cells, integral optical density (IOD), optical density (OD) *per* pixel and viability and necrosis areas. Sections were mounted for examination. Stained slides were imaged at 0.25 μm *per* pixel resolution using a ScanScope XT.

Statistical analysis

All results (except temperature measurements, which comprise single observations) are expressed as the average of three independent experiments ± SEM. For statistical analysis of cell proliferation and biodistribution studies one way ANOVA followed by Bonferroni test were performed. Differences were considered significant when $P < 0.05$.

3. Results

The in vitro studies demonstrated different patterns of BPA uptake for each cell line. Figure 1 shows the cellular boron uptake in the three human melanoma cell lines (A375, MEL-J and M8) as a function of time. MEL-J and A375 cells showed a time-dependent

increase in the intracellular boron concentration reaching a maximum value at 4 hours of incubation, with a non significant slight increase at 24 hours. On the other hand, the boron concentration did not show significant changes during the elapsed time of the study in the M8 cells. At 4 hours, the BPA average uptake was 0.119 ± 0.016 μg B/10^6 cells for MEL-J, 0.109 ± 0.007 μg B/10^6 cells for A375 and 0.035 ± 0.007 μg B/10^6 cells for M8 cells (*** $P < 0.001$ for MEL-J and A375 vs. M8 cells). The BPA uptake for MEL-J was 1.09 and 3.40 times higher than for A375 and M8, respectively, showing selectivity in the BPA uptake for this cell line.

Table 1 show the results of the biodistribution of BPA at a dose of 350 mg/kg in NIH nude mice bearing melanoma. Tumor showed a maximum average BPA concentration of 25.9 ± 2.6 μg/g, with individual values ranging between 11.7 and 52.0 μg/g of ^{10}B at 2 h post-injection. Tumor-to-blood and tumor-to-distal skin ratios were 4.3 and 2.5, respectively.

The average temperature of the left flank, determined by SIRI, was always around 37 ºC, a value close to body core temperature, also measured independently by a thermocouple in the right groin. The temperature of the normal skin surrounding the tumor on the right flank (inoculated side) was usually higher (about 40 ºC) during the first two weeks after inoculation, and then approached 37-38 ºC after two weeks. Tumors started to be observed in the thermograhic studies around this point, and their temperature always decreased as the tumors increased in size, with values ranging between 37 ºC and 23 ºC.

Figure 2A shows the tumor temperature for each mouse measured in three separate days during the week previous to the biodistribution study, as a function of the later measured Tumor-to-Blood (T/B) ratios. Error bars are representative of the overall infrared camera accuracy (± 0.3 ºC). A significant correlation between tumor temperature and T/B boron concentration ratio was found (R-square=0.7, rational function fit). Low temperature tumors, (usually tumors with a size of more than 1 centimetre), are associated with low T/B ratios. Conversely, tumors with higher temperature (not necessarily small in size), are found to concentrate more ^{10}B relative to blood. These findings can be better interpreted with the presentation of the data as shown in Figure 2B. Disregarding inflammation or metabolic heat sources, the difference between body core temperature (Tcore) and tumor temperature (Ttum), which represents the temperature drop through the tumor, is proportional to tumor thickness and inversely proportional to tumor heat conductivity. Thus, smaller tumors or tumors with higher heat conductivity (or both) would present smaller differences. In this study, tumors with smaller temperature differences are precisely those that accumulated more boron relative to blood.

The histologic studies showed tumors with wide areas of viability (Fig. 3A) and variable number of small *foci* of necrosis (Fig. 3B). The percentage of viability area for each tumor sample was measured as a function of the boron uptake. Tumors with large areas of viability presented high boron uptake values (Fig. 3C).

The immunohistochemical studies revealed, in tumors with extensive areas of viability, a high number of Ki-67-positive cells. Furthermore, we found tumor blood vessels of large diameter in the peripheral zone of the tumor as evidenced by the expression of the

endothelial marker CD31. Figures 4A to D show two different samples: the case with the highest mark for both antibodies (Ki-67 and CD31) and the case with the lowest mark for both of them.

In order to evaluate whether a direct correlation between proliferation status and BPA uptake exists, a non-dimensional quantity, computed as the scored number of Ki-67 positive cells, times the average optical density (IOD) was constructed. This overall quantity, referred to as Proliferation Density (PD), was used as an independent variable and it was compared against the difference between boron concentration in tumor and blood boron concentration. The rationale for adopting the latter is as follows: in a very simplified tumor uptake model, it can be assumed that BPA reaches tumor cells first by passive diffusion and, depending on the cell metabolism, then it can be uptaken actively by those cells that are in the active state of the cell cycle (G1, S, G2, M), increasing further their boron concentration, but not by cells in quiescent state (G0, no proliferation). Following this idea, it is proposed that $C_{tum} = C_{blood} + C_{act}$, where C_{act} is the contribution to the total tumor concentration by active (proliferating) cells.

Figure 5 shows the values of PD (in arbitrary units) and the corresponding C_{act}, using the minimum boron concentration, estimated after measuring around five to seven pieces in each tumor, as the value for C_{tumor}. The reason for choosing the minimum boron concentration in tumor is based on the fact that tumor control probabilities in the presence of non-uniform dose distributions (such as those typically observed in the BNCT clinical setting) are strongly influenced by the minimum rather than the average dose. A logistic curve with two free parameters and passing through (0,0) was employed for fitting the experimental values, providing a suitable empirical relationship that

relates both quantities and offers the possibility of further studies and interpretations of the data.

Discussion

The usefulness of BNCT in the treatment of some types of malignant melanoma has convened a lot of multidisciplinary groups in order to optimize the outcome of this therapy in different research centers around the world. In our laboratory, and with the objective of improving the efficacy of BNCT for the treatment of melanoma, we have evaluated several physical, structural and histological parameters in an animal model, aiming at demonstrating the possibility of applying BNCT but considering individual patient's characteristics.

Standard radiotherapy shows different responses for the same kind of tumor (7). It has been observed that patients with the same histopathological diagnosis of cutaneous melanoma had different clinical outcomes to identical BNCT protocols (16). Interestingly, it has been observed that even tumors located in the same leg of one patient showed a different grade of response to the same treatment (6).

There are different ways to optimize the BNCT treatment. The synthesis of new boron agents with more boron atoms per molecule or specific compounds for each kind of tumor is certainly one of them. Moreover, the development of new neutron sources and appropriate beams in accordance with tumor localization is a mode of improving the efficacy of BNCT. The use of radiosensitizing drugs in combination with the BNCT reaction have been studied by some groups including our laboratory in differents

pathologies (17, 18). In this work, and in agreement with the new tendency of personalized oncology, we attempted to develop a series of different appropriate tests for the design of new screening protocols applicable prior to a BNCT treatment for each individual patient and lesion. As a first neccessary step, with this goal in mind, we evaluated the boronated amino acid (BPA) incorporation both in vitro as in vivo. After that, we performed predictive curves of tumoral uptake of BPA versus different physical and biological characteristics of each tumor. A previous estimation of the amount of boron in the tumor would allow optimization of the delivered treatment plan.

In this study we demonstrated the differential kinetic uptake of BPA in three human melanoma cell lines. The BPA incorporation was higher for two of them (MEL-J and A375 vs. M8) and MEL-J cells showed the fastest uptake kinetic with a peak at 4 h after incubation other compared to A375 cells. Different intracellular boron concentrations for distinct cell lines of other tumor types were published as well (19, 20).

The subsequent in vivo studies with one of the cell lines implanted into the flank of nude mice showed an exponential tumor growth after 25 days of implantation of 4 10^6 cells reaching a volume of 930 mm^3 (results not shown). The BPA biodistribution exhibited a peak of boron in the tumor at 2 h post-administration with individual values ranging between less than 12 ppm and no more than 52 ppm. In some animals the ratios were higher than 3, which is a generally accepted ratio for a therapeutic BNCT application. In others, the boron tissue ratios obtained were lower than 3. This is in agreement with other results published in different experimental studies. It is worth to note that, as in other animal models, the kidney has a high boron concentration, since it is the excretion route of BPA and its metabolites (21). In this work we aimed to detect

possible correlations between BPA uptake, temperature and the histological composition of the tumor sample. A direct correlation between tumor boron uptake and core-to-tumor temperature differences (a measure of heat flux across the tumor and tumor heat production) was observed. We also observed that tumors with small necrotic areas exhibited higher boron uptake and temperature than tumors with large necrotic regions.

In xenograft models, generally, tumors grow very rapidly and their vasculature is significantly different from that of normal tissue. Tumor vessels are small, poorly organized, hyperpermeable and with impaired blood supply. All of these features contribute to reduce the tumor temperature (21). On the other hand in terms of material composition, soft tissues can be thought of as composed of mainly three physical materials: water, fat and protein. Among these, water is the material with the highest heat conductivity, being protein the worst conducting one. Thus, tumors with higher water content in the vascular, interstitial or stromal compartments will conduct heat more efficiently. Heat sources, as those originating from metabolism or inflammation, will always produce higher tumor temperatures (or, again, smaller differences relative to core temperature). Since they can be considered as additional factors that could play a positive role in boron uptake, they will affect the observed temperature in the same direction as decreasing tumor size and increasing water content (22). It is interesting to note that some studies have demonstrated that mouse tumor xenografts have a slightly lower temperature than the surrounding normal tissue as tumor grows (16). The same behaviour was observed in the present study.

Thermal imaging has been used in clinical medicine since early 1960. This technique has been applied in the evaluation of patients suspected of having breast cancer, where an abnormal thermal pattern can be detected prior to clinical or mammographic changes. Also dynamic thermal imaging has been used intraoperatively during neurosurgical interventions (23). If our results were confirmed in human biodistribution studies for cutaneous melanoma, infrared thermography could provide a prospective tool for assessing non-invasively and beforehand the possible differences in boron tumor uptake and thus contribute to personalize a BNCT treatment plan.

In immunohistochemical studies two different markers were analysed: Ki-67 and CD31. The Ki-67 protein is a cellular marker of proliferation that is presented in the cell in G1, S, G2 and mitosis cell cycle phases but it is absent in G0. Sometimes the degree of proliferative activity is considered to be one of the most important characteristics of malignant cutaneous melanoma when compared with benign melanocytic lesions (24, 25). Our in vivo studies showed that Ki-67 could be an indicator of the degree of boron active incorporation in solid tumors. This fact is important not only to select a patient candidate for BNCT, but also to improve the clinical outcome of the therapy. Although more data would be needed to confirm both low and high proliferation density behaviour regarding active BPA uptake, the fact that a good fitting was obtained with a sigmoid curve that exhibits asymptotic trend for high proliferation values could indicate a possible saturation mechanism, with maximum achievable boron concentration values in tumor and, on the other hand, boron uptake similar to blood concentration values in quiescent cells. A similar correlation was found in the work of Coderre et al., analysing cell density and boron concentration (26). A quantity referred to as “cellularity index”, was determined by stereological measurements of glioblastoma samples, and it was

considered an estimate of the density of tumor cells. When plotted against boron concentration, the data exhibited a linear correlation that increased with the cellularity index of each particular sample. In the present work, an additional factor is considered, i.e., the Ki-67 staining intensity which, together with cell counting provides a more suitable index for the tumor proliferative state.

In the case of CD31 staining, which is a specific marker of vascular endothelial cells, two different patterns were observed: tumors with a high number of large cross-section vessels and tumors with small vessels. The first type of tumors showed a higher boron uptake compared to the other type of tumors, with a smaller number of vessels. However, the importance of tumor vascularization for the prognosis of primary malignant melanomas of the skin remains controversial (27, 28). With these results obtained in an animal model of melanoma, we could suggest that tumors with larger blood supply also positively correlate with higher tumor temperatures.

In summary, and in agreement with the personalized medicine, a new approach for optimizing the BNCT application is proposed. The main idea is to provide a treatment plan according to each patient's individual characteristics based on *a priori* knowledge of the genetic variation and specific characteristics of each patient tumor.

Acknowledgments

This work was partially supported by Grant PAE 22393, ANPCyT and by INVAP SE.

References

1. Bandarchi B, Jabbari CA, Vedadi A, Navab R. Molecular biology of normal melanocytes and melanoma cells. *J Clin Pathol* 2013; 66: 644-648.

2. Barth RF, Coderre JA, Vicente MG, Blue TE. Boron neutron capture therapy of cancer: current status and future prospects. *Clin Cancer Res* 2005; 11: 3987-4002.

3. Barth RF, Vicente MG, Harling OK, *et al*. Current status of boron neutron capture therapy of high grade gliomas and recurrent head and neck cancer. *Radiat Oncol* 2012;7:146.

4. Mishima Y, Ichihashi M,, Hatta S, *et al*. New thermal neutron capture therapy for malignant melanoma: melanogenesis-seeking IOB molecule-melanoma cell interaction from in vitro to first clinical trial. *Pigm Cell Res* 1989; 2:226-234.

5. Madoc-Jones H, Zamenhof R, Solares G, *et al.* A phase I dose escalation trial of boron neutron capture therapy for subjetcs with metastatic subcutaneous melanoma of the extremities. In: Mishima Y, editor. Cancer neutron capture therapy. New York and London: Plenum Press; 1996 p.707-16.

6. Fukuda H, Honda C, Wadabayashi N, Kobayashi T, *et al*. Pharmacokinetics of 10B-p-boronophenylalanine in tumours, skin and blood of melanoma patients: a study of boron neutron capture therapy for malignant melanoma. *Melanoma Res* 1999; 9:75-83.

7. Menendez P, Roth B, Pereira M, *et al*. BNCT for skin melanoma in extremities: updated argentine clinical results. *Appl Rad Isot* 2009;67: S50-S53.

8. Pawlik T and Keyomarsi K. Role of cell cycle in mediating sensitivity to radiotherapy. *Int J Radiation Oncol Biol Phys* 2004;59: 928-942.

9. Chan IS, Ginsburg GS. Personalized medicine: progress and promise. *Annu Rev Genomics Hum Genet* 2011; 12:217-244.

10. Guerra L, Mordoh J, Slavutsky I, *et al.* Characterization of IIB-MEL-J: a new and highly heterogenous human melanoma cell line. *Pigment Cell Research* 1989;2:504-509.

11. US Department of Health and Human Services. Guide for the care and use of laboratories animals. Public Health Service, National Institute of Health; 1985. NIH Publication 86-23.

12. Lee YS, Bulliard D, Zalutsky M. Therapeutic efficacy of antiglioma mesenchymal extracellular matrix 131 I-radiolabeled murine monoclonal antibody in a human glioma xenograft model. *Cancer Res* 1998; 48:559-565.

13. Coderre J, Chanana A, Joel D, *et al*. Biodistribution of boronophenylalanine in patients with glioblastoma multiforme: boron concentration correlates with tumor cellularity. *Radiat Res* 1998;149:163-170.

14. Santa Cruz, G., González S, Dagrosa, A, Schwint A, *et al*. Dynamic infrared imaging for biological and medical applications in Boron neutron capture therapy. In: M. Safai, J. Brown (eds.), Thermosense: Thermal Infrared Applications XXXIII, Proceedings of SPIE . 8013 SPIE, Bellingham, WA, 2011.

15. Brandizzi D, and Cabrini RL Microspectrophotometric quantitation of immunohistochemical reactions by image analysis. *Acta Microscopica* 2013; 22:1-3.

16. Gonzalez S, Bonomi M, Santa Cruz G, *et al*. First BNCT treatment of a skin melanoma in Argentina: dosimetric analysis and clinical outcome. *Appl Radiat Isot* 2004;61: 1101-1105.

17. Perona M, Rodríguez C, Carpano M, *et al*. Improvement of the boron neutron capture therapy (BNCT) by the previous administration of the histone deacetylase inhibitor sodium butyrate for the treatment of thyroid carcinoma. *Radiat Envir Biophys* 2013;52:363-73.

18. Hiramatsu R, Kawabata S, Miyatake S, Kuroiwa T, Easson MW, Vicente MG. Application of a novel boronated porphyrin (H_2OCP) as a dual sensitizer for both PDT and BNCT. Lasers Surg Med 2011;43:52-8.

19. Sun T, Zhou Y, Xie X, *et al*. Selective uptake of boronophenylalanine by glioma stem/progenitor cells. *Appl Radiat Isot* 2012;70:1512-1518.

20. Ferrari C, Zonta C, Cansolino L, *et al*. Selective uptake of p-boronophenylalanine by osteosarcoma cells for boron neutron capture therapy. *Appl Radiat Isot* 2009;67: S341-4.

21. Song C, Appleyard V, Murray K, *et al.* Thermograhic assessment of tumor growth in mouse xenografts. *Int J Cancer* 2007;121:1055-1058.

22. Funda DP, Houstek J, Holub M, *et al*. Differences in thermoregulation between inmunocompetent and immunodeficient hairless mice exposed to mild cold. *Folia Microbiol* 1998;43:487-489.

23. Lloyd-Williams K, Handley RS. Infra-red thermometry in the diagnosis of breast disease. *Lancet* 1961;2:1378-1381.

24. Rieger E, Hoffman Wellenhof R, *et al*. Comparison of roliferative activity as assessed by proliferating cell nuclear antigen (PCNA) and Ki 67 monoclonal antibodies in melanocityc skin lesions. *J Cutan Pathol* 1993;20:229-236.

25. Vogt T, Zipperer K, Vogt A, *et al.* P53 protein and Ki 67 antigen expression are both reliable biomarkers of prognosis in thick stage I nodular melanomas of the skin. *Histopathology* 1997; 30:57-63.

26. Coderre J, Chanana A, Joel D, *et al*. Biodistribution of boronophenylalanine in patients with gioblastoma mltiforme: boron concentration correlates with tumor cellularity. *Radiation Research* 1998;149:163-170.

27. Eichhoff O, Zipser M, Xu M, *et al*. The inmunohistochemistry of invasive and proliferative phenotype swiching in melanoma: a case report. *Melanoma Res* 2010;20:349-355.

28. Kuzu I, Bicknell R, Harris A, *et al*. Heterogenity of vascular endothelial cells with relevance to diagnosis of vascular tumors. *J Clin Pathol* 1992;45:143-148.

Legends of the figures

Figure 1: Cellular boron uptake in the three human melanoma cell lines (A375, MEL-J and M8) after 0.5, 1, 2, 4 and 24 h of incubation with BPA (50 ppm ^{10}B). After 4 h of incubation, the ratios MEL-J/M8 and A375/M8 were 3.40 and 2.73, respectively. Each point is the average of three independent experiments ± SEM. ***, $P < 0.001$ for MEL-J *vs.* M8 and A375 *vs.* M8 at 24 hours.

Figure 2A: Tumor temperature vs. T/B ratio, for different animals. Temperature measurements using SIRI were taken prior to the biodistribution studies, between one week and one day before. A significant correlation between tumor temperature and T/B boron concentration ratio was found (R-square=0.7, rational function fit).

Figure 2B: Body core temperature minus tumor temperature vs. T/B ratio. Again, a significant correlation (R-square: 0.76, rational function fit) was observed, slightly better than T_{tum} vs. T/B. Neglecting inflammation or metabolic sources, the difference between body core temperature (T_{core}) and tumor temperature (T_{tum}) represents the temperature drop through the tumor, which is proportional to tumor thickness and inversely proportional to heat conductivity. If other heat sources were present, this difference would always decrease and it can be even negative (tumor temperature higher than 37 ºC). In the present experimental set-up, it cannot be possible to uncouple both contributions, unless dynamic infrared studies are employed, which esentially exploit transient changes to determine both heat difussivity (related with the characteristic time for temperature recovery) and heat sources (associated with the asymptotic temperature after recovery).

Figure 3A: Hematoxylin and eosin stained tumour section. (40X). Tumor with large areas of viability. One representative image from 10 mice per group.

Figure 3B: Hematoxylin and eosin stained tumour section. Extensive areas of necrosis are highlighted in the tumor section with black arrows. (40X)**.** One representative image from 10 mice per group.

Figure 3C: Percentage of tumor viability vs. boron uptake (ppm) in different samples. The tumors with large areas of viability presented high boron concentrations.

Figure 4 A-D: Ki-67 and CD31 stains, each performed on histological sections of tumor samples of higher boron concentrations (left panel) and lower boron uptake (right panel) (20X).

Figure 5: "Active" minimum boron concentration (i.e., the difference between minimum tumor boron concentration minus blood boron concentration) vs. Proliferation Density, PD, for different tumors. Vertical error bars represent the experimental uncertainty in boron measurements and horizontal error bars are the result of adding in quadratures the errors for cell counting (observer cell selection, set to 10% as a conservative estimate) and IOD standard deviation. According to the simple interpretation of the tumor-minus-blood difference that accounts for active BPA uptake, it is assumed that for very low PD values (almost no active cells) this difference should approach zero and that, in the other extreme, saturation in active BPA uptake would

take place. Under these assumptions, a logistic curve was employed, with the constraint that it must pass through the (0,0).

Table 1: Boron concentration in the different tissues of NIH nude mice bearing human melanoma (MEL-J). The measurements were performed at different times after BPA injection at a dose of 350 mg/Kg b.w. The values are the average ± SEM of 12 separate biodistribution studies with n = 10 mice per experimental group. **, $P < 0.01$; ***, $P < 0.001$.

Table 1

Tissue	0.5 h	1 h	2 h	3 h
Tumor	15.8 ± 2.3 (5.4-24.0)	22.3 ± 1.9** (13.9-28.2)	**25.9 ± 2.6*** (11.7-52.0)**	19.8 ± 2.5 (3.1-33.5)
Blood	7.2 ± 1.2 (4.8-9.1)	8.8 ± 1.9 (3.9-15.0)	**6.0 ± 1.7 (2.2-14.0)**	3.5 ± 1.0 (1.6-5.0)
Distal Skin	10.9 ± 1.6 (7.0-15.7)	12.2 ± 2.2 (5.7-23.0)	**10.4 ± 2.3 (3.7-25.0)**	8.6 ± 2.3 (2.9-21.9)
Surrounding Skin	11.2 ± 2.0 (6.5-22.6)	15.3 ± 2.4 (8.1-36.4)	13.0 ± 2.3 (3.0-23.6)	10.9 ± 2.8 (2.9-31.1)
Liver	10.4 ± 2.4 (2.2-22.5)	8.6 ± 1.4 (5.9-13.5)	6.8 ± 1.6 (3.1-15.1)	4.5 ± 1.3 (2.4-7.4)
Spleen	14.1 ± 2.5 (3.9-29.1)	13.7 ± 2.0 (8.4-24.2)	13.4 ± 2.8 (6.1-34.9)	7.1 ± 2.0 (2.9-16.6)
Kidney	27.3 ± 3.1 (17.4-43.4)	33.5 ± 2.7 (21.5-46.9)	17.3 ± 2.6 (7.1-35.6)	14.9 ± 3.3 (6.1-48.5)
Lung	12.1 ± 1.9 (3.5-16.4)	11.3 ± 1.7 (6.5-17.7)	8.7 ± 2.3 (3.1-28.7)	6.0 ± 1.8 (3.5-16.1)

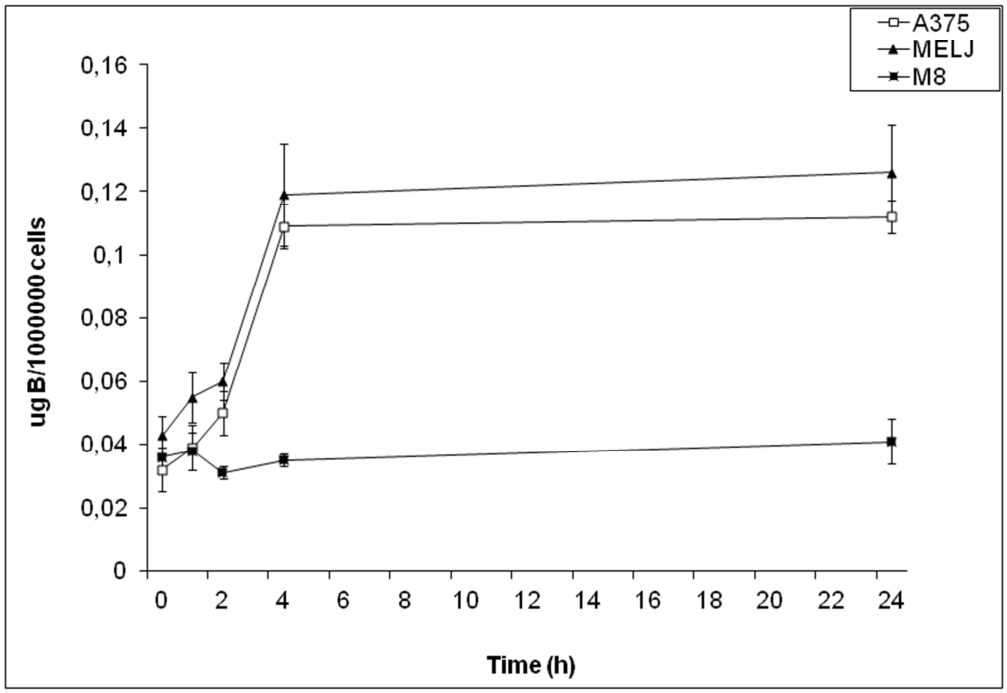

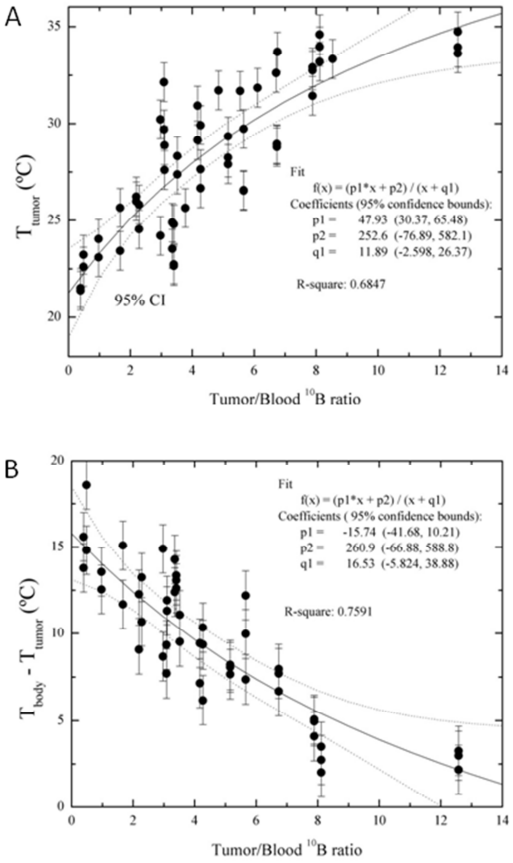

A

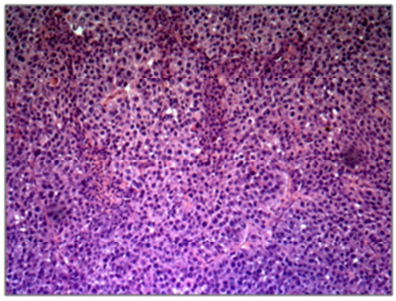

B

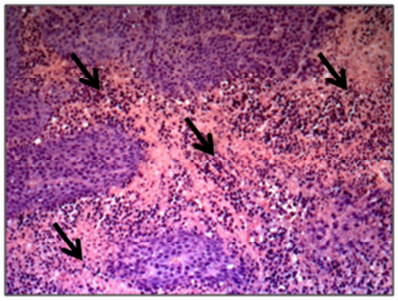

C